ELSEVIER

J. Non-Newtonian Fluid Mech. 147 (2007) 189–199

Journal of Non-Newtonian Fluid Mechanics

www.elsevier.com/locate/jnnfm

A simple method for simulating general viscoelastic fluid flows with an alternate log-conformation formulation

Oscar M. Coronado [a], Dhruv Arora [a], Marek Behr [a,b], Matteo Pasquali [a,*]

[a] *Department of Chemical and Biomolecular Engineering and Computer and Information Technology Institute, Rice University, MS 362, 6100 Main Street, Houston, TX 77005, USA*

[b] *Chair for Computational Analysis of Technical Systems (CATS), CCES, RWTH Aachen University, Aachen 52056, Germany*

Received 19 March 2007; received in revised form 12 July 2007; accepted 18 August 2007

Abstract

The log-conformation formulation has alleviated the long-standing high Weissenberg number problem associated with the viscoelastic fluid flows [R. Fattal, R. Kupferman, Constitutive laws for the matrix-logarithm of the conformation tensor, J. Non-Newtonian Fluid Mech. 123 (2004) 281–285]. This formulation ensures that solutions of viscoelastic flow problems are physically admissible, and it is able to capture sharp elastic stress layers. However, the implementations presented in literature thus far require changing the evolution equation for the conformation tensor into an equation for its logarithm, and are based on loosely coupled (partitioned) solution procedures [M.A. Hulsen, et al., Flow of viscoelastic fluids past a cylinder at high Weissenberg number: stabilized simulations using matrix logarithms, J. Non-Newtonian Fluid Mech. 127 (2005) 27–39]. A simple alternate form of the log-conformation formulation is presented in this article, and an implementation is demonstrated in the DEVSS-TG/SUPG finite element method. Besides its straightforward implementation, the new log-conformation formulation can be used to solve all the governing equations (continuity, conservation of momentum and constitutive equation) in a strongly coupled way by Newton's method. The method can be applied to any conformation tensor model. The flows of Oldroyd-B and Larson-type fluids are tested in the benchmark problem of a flow past a cylinder in a channel. The accuracy of the method is assessed by comparing solutions with published results. The benefits of this new implementation and the pending issues are discussed.

Keywords: DEVSS-TG/SUPG; Log-conformation; Oldroyd-B model; Larson model; Flow past a cylinder in a channel

1. Introduction

In the past two decades, considerable effort has been given to the development of robust and stable numerical methods for simulating complex flows of complex fluids, which pose several numerical challenges. Such extensive research is motivated by many industrial applications and scientific importance of complex fluids (fluids with inherent micro–macro structure such as polymer solutions and melts, inks, paints, or blood).

Like for Newtonian fluids, the flow of complex fluids is governed by the conservation of mass and momentum equations; for cost-effective simulations, coarse-grained constitutive models are used to relate the fluid stresses with the rate-of-strain. The most commonly used constitutive models involve a hyperbolic partial differential equation that represents the transport of the elastic stress or conformation tensor, a physical quantity which represents the local state of the fluid [1]. The conformation must be positive-definite at all stages of the simulation, because its eigenvalues and eigenvectors represent the local straining and orientation of the microconstituents.

The ratio of the relaxation time and the time associated with the local rate of deformation—the Weissenberg number Wi—is the key dimensionless number in these simulations. In all early efforts of viscoelastic fluid flow simulations, the numerical methods yielded mesh-converged results only up to a critical value of Wi; this is referred to as the high Weissenberg number problem (HWNP), where the smoothness of viscoelastic stresses should be expected to deteriorate [2]. In flows with smooth boundaries, the HWNP is related to the development of steep internal layers of conformation, and their poor representation by interpolation functions based on low-order polynomial [3]. Recently, a logarithmic representation of the conformation tensor (log-conformation formulation) was proposed by Fattal and Kupferman [3,4]; this representation ensures

* Corresponding author. Tel.: +1 713 348 5830; fax: +1 713 348 5478.
E-mail address: mp@rice.edu (M. Pasquali).

0377-0257/$ – see front matter © 2007 Elsevier B.V. All rights reserved.
doi:10.1016/j.jnnfm.2007.08.005

the positive definiteness of the conformation tensor, and captures well steep layers which are exponential in nature. Hulsen et al. [5] showed that the log-conformation formulation improves the stability of numerical methods by applying the DEVSS/DG method to simulate the flow of Oldroyd-B fluid and Giesekus fluid past a cylinder in a channel. Similar results were shown by Kwon [6] in the flow of a Leonov fluid through a 4:1 contraction. In both cases, physically realistic results could be computed at considerably higher Wi than previously reported.

In this work, a simpler, yet comparably effective, method to implement the log-conformation formulation in the finite element context is presented. The DEVSS-TG/SUPG method [7] is used to demonstrate its performance and easy implementation. The principal advantage of this method is that the original code remains unchanged; the chief difference is that the conformation tensor $\mathbf{M}$ is substituted by $\exp \mathbf{S}$, where $\mathbf{S} \equiv \log \mathbf{M}$ becomes the new unknown of the problem. The method is tested using the benchmark problem of an Oldroyd-B fluid flow past a cylinder in a rectangular channel, obtaining an increase of 40% in the maximum Wi with respect to the original DEVSS-TG/SUPG method.

The generality of the proposed log-conformation formulation is demonstrated by using the Larson-1 and Larson-2 models [18], obtaining an increase in the maximum Wi of a factor of 3 and 24%, respectively. Although the proposed method gives an increased stability range of Wi, the accuracy cannot be demonstrated beyond a critical Wi, which in the case of Oldroyd-B fluid is ~ 0.7 (also observed in Refs. [5,12]).

This article is organized as follows. The governing equations are presented in Section 2 followed by a review of the existing log-conformation formulations in Section 3. The proposed DEVSS-TG/SUPG log-conformation formulation and the numerical issues associated with its implementation are presented in Section 4. The numerical results for the problem of an Oldroyd-B fluid past a cylinder in a rectangular channel are presented in Section 5, followed by a 1-D analysis to study the differences observed between different log-conformation formulations in Section 6. The generality of the proposed log-conformation formulation is demonstrated for the Larson-1 and Larson-2 models in Section 7, and finally, the conclusions and discussions are presented in Section 8.

2. Equations governing the flow of viscoelastic fluids

The steady inertialess flow of an incompressible viscoelastic fluid occupying a spatial domain Ω with boundary Γ is governed by the conservation of momentum and continuity equations,

$$\nabla \cdot \mathbf{T} = \mathbf{0} \quad \text{on } \Omega, \tag{1}$$

$$\nabla \cdot \mathbf{v} = 0 \quad \text{on } \Omega, \tag{2}$$

where $\mathbf{T} = -p\mathbf{I} + \boldsymbol{\tau} + \boldsymbol{\sigma}$ is the stress tensor, $\mathbf{v}$ the fluid velocity, p the pressure, $\mathbf{I}$ the identity tensor, $\boldsymbol{\tau} = 2\eta_s \mathbf{D}$ the viscous stress, η_s the solvent viscosity, $\mathbf{D} \equiv (\mathbf{L} + \mathbf{L}^T)/2$ the rate-of-strain tensor, and $\boldsymbol{\sigma}$ is the elastic stress. The variable $\mathbf{L}$ represents the traceless velocity gradient [7],

$$\mathbf{L} = \nabla \mathbf{v} - \frac{1}{\operatorname{tr} \mathbf{I}} (\nabla \cdot \mathbf{v}) \mathbf{I}, \tag{3}$$

where tr denotes trace.

Eqs. (1)–(3) reach a closed form when a suitable constitutive model is used to relate $\boldsymbol{\sigma}$ to the flow variables. Pasquali and Scriven [8] presented a generalized constitutive model in terms of the conformation tensor $\mathbf{M}$,

$$-\mathbf{v} \cdot \nabla \mathbf{M} + 2\xi \frac{\mathbf{D} : \mathbf{M}}{\mathbf{I} : \mathbf{M}} \mathbf{M} + \zeta \left(\mathbf{M} \cdot \mathbf{D} + \mathbf{D} \cdot \mathbf{M} - 2 \frac{\mathbf{D} : \mathbf{M}}{\mathbf{I} : \mathbf{M}} \mathbf{M} \right) + \mathbf{M} \cdot \mathbf{W} + \mathbf{W}^T \cdot \mathbf{M} \underbrace{- (1/\lambda)(g_0 \mathbf{I} + g_1 \mathbf{M} + g_2 \mathbf{M}^2)}_{\mathbf{FM}} = \mathbf{0}, \tag{4}$$

where $\xi(\mathbf{M})$ and $\zeta(\mathbf{M})$ are the polymer compliance to stretching and orientations, respectively; $\mathbf{W} \equiv (\mathbf{L} - \mathbf{L}^T)/2$ is the vorticity tensor; $g_0(\mathbf{M})$, $g_1(\mathbf{M})$ and $g_2(\mathbf{M})$ are relaxation functions and λ is the characteristic relaxation time.

The elastic stress $\boldsymbol{\sigma}$ is related to $\mathbf{M}$ as

$$\boldsymbol{\sigma} = 2\xi \frac{\mathbf{M}}{\mathbf{I} : \mathbf{M}} \mathbf{M} : \frac{\partial a}{\partial \mathbf{M}} + 2\zeta \left(-\frac{\mathbf{M}}{\mathbf{I} : \mathbf{M}} \mathbf{M} : \frac{\partial a}{\partial \mathbf{M}} + \mathbf{M} \cdot \frac{\partial a}{\partial \mathbf{M}} \right), \tag{5}$$

where $a(\mathbf{M})$ is the Helmholtz free energy per unit volume of the complex fluid. Different constitutive models are given by the proper selection of the constitutive functions ξ, ζ, g_0, g_1, g_2 and a (a detailed description can be found in Ref. [8]).

Boundary conditions on the momentum equation are needed on the entire boundary $\Gamma = \Gamma_g \cup \Gamma_h$. Boundary conditions on velocity and momentum flux (traction) are given by

$$\mathbf{v} = \mathbf{g} \quad \text{on } \Gamma_g, \tag{6}$$

$$\mathbf{n} \cdot \mathbf{T} = \mathbf{h} \quad \text{on } \Gamma_h, \tag{7}$$

where $\mathbf{g}$ and $\mathbf{h}$ are given functions, and $\mathbf{n}$ is the outward unit vector normal to the boundary.

3. The log-conformation formulation

The log-conformation formulation was recently proposed by Fattal and Kupferman [3]; in this method, the constitutive equation is written in terms of the logarithm of the conformation tensor $\mathbf{S} \equiv \log \mathbf{M}$. This change of variable ensures the positive-definiteness of $\mathbf{M}$, and it is able to capture better sharp layers at high Wi due to the exponential nature of the transformation. Flow problems are solved by discretizing the governing equations, e.g., with the finite difference method [4].

The log-conformation formulation was first implemented in finite element context by Hulsen et al. [5]. The constitutive equation was written in terms of $\mathbf{S}$, and DEVSS/DG was applied to solve the benchmark flow of an Oldroyd-B and Giesekus fluid past a cylinder in a channel. The logarithm of $\mathbf{M}$ can be computed easily in its principal co-ordinate system, where the eigenvalues of $\mathbf{M}$ give the stretches m_i in the principal directions and its eigenvectors give the principal directions $\mathbf{n}_i$, $i = 1, 2, 3$, thus

$\mathbf{S} = \log \mathbf{M} = \sum_{i=1}^{3} \log(m_i)\mathbf{n}_i\mathbf{n}_i = \sum_{i=1}^{3} s_i \mathbf{n}_i\mathbf{n}_i$, where $s_i = \log m_i$ are the principal values of $\mathbf{S}$, and whose existence is always guaranteed because the m_i are always positive.

Hulsen et al. [5] presented results for Oldroyd-B and Giesekus models for which $\xi = \zeta = 1$ (the molecules undergo affine deformations); a generalized form applicable to any conformation tensor model [8] is presented here, following the derivation in Ref. [5],

$$\mathbf{v}\cdot\nabla\mathbf{S} = \sum_{i=1}^{3}\left[\frac{2(\xi-\zeta)}{\sum_{j=1}^{3} m_j}\sum_{j=1}^{3} d_{jj}m_j + 2(\zeta d_{ii} + w_{ii}) + \frac{f_i}{m_i}\right]\mathbf{n}_i\mathbf{n}_i + \sum_{\substack{i=1\\ i\neq j}}^{3}\sum_{j=1}^{3}\frac{s_i - s_j}{m_i - m_j}[\zeta(m_i - m_j)d_{ij} + m_i w_{ij} + m_j w_{ji}]\mathbf{n}_i\mathbf{n}_j, \tag{8}$$

where d_{ij} and w_{ij} are respectively the components of the rate-of-strain and vorticity tensors in the basis defined by the principal directions $\mathbf{n}_i$. The molecular relaxation contribution $\mathbf{F}(\mathbf{M})$, given by the last term in Eq. (4), is an isotropic function; therefore, its components f_i in the principal directions $\mathbf{n}_i$ are

$$f_i = -\frac{1}{\lambda}(g_0 + g_1 m_i + g_2 m_i^2). \tag{9}$$

Following the approach of Ref. [5], the implementation of the generalized log-conformation formulation requires:

(1) Solution of the continuity and momentum equations in the laboratory co-ordinate system at fixed $\boldsymbol{\sigma}$;
(2) Transformation of $\mathbf{D}$ and $\mathbf{W}$ from the laboratory co-ordinate system to the co-ordinate system identified by the eigenvectors of $\mathbf{M}$;
(3) Solution of Eq. (8) in the co-ordinate system of the eigenvalues of $\mathbf{M}$;
(4) Back-transformation of $\mathbf{M}$ to the laboratory co-ordinate system; and
(5) Computation of $\boldsymbol{\sigma}$ from $\mathbf{M}$ in the laboratory co-ordinate system.

The log-conformation formulation improves the stability of the numerical method at high Wi [3,5,6]. Presumably, the iterative procedure outlined above will become increasingly inefficient in problems with large "non-diagonal" coupling, e.g., free surface flows at low capillary number and viscoelastic flows at low value of the solvent viscosity. In these cases, fully coupled procedures are more robust and efficient [7,9]. Coupled solution techniques require casting and discretizing all the differential equations in the same co-ordinate system, and solving the resulting coupled algebraic equations with a non-linear solver, e.g., Newton's method.

Such a method is proposed below. It casts and solves in a coupled way the viscoelastic flow equations in generalized conformation tensor form by applying the log-conformation change of variable.

4. The DEVSS-TG/SUPG log-conformation formulation and the numerical issues associated with its implementation

In the present work, a simpler implementation of the log-conformation formulation in a finite element context is presented. Although its application is only demonstrated in the DEVSS-TG/SUPG method [7], it can be easily applied to any other method as well, e.g., `GLS4` [10]. The variable $\mathbf{S}$ is introduced by replacing $\mathbf{M}$ with $\exp\mathbf{S}$ in Eq. (4). The transformed Eq. (4) is

$$-\mathbf{v}\cdot\nabla(\exp\mathbf{S}) + 2\xi\frac{\mathbf{D}:(\exp\mathbf{S})}{\mathbf{I}:(\exp\mathbf{S})}(\exp\mathbf{S}) + \zeta\left[(\exp\mathbf{S})\cdot\mathbf{D} + \mathbf{D}\cdot(\exp\mathbf{S}) - 2\frac{\mathbf{D}:(\exp\mathbf{S})}{\mathbf{I}:(\exp\mathbf{S})}(\exp\mathbf{S})\right] + (\exp\mathbf{S})\cdot\mathbf{W} + \mathbf{W}^T\cdot(\exp\mathbf{S}) - \frac{1}{\lambda}(g_0\mathbf{I} + g_1(\exp\mathbf{S}) + g_2(\exp\mathbf{S})^2) = \mathbf{0}. \tag{10}$$

4.1. The DEVSS-TG/SUPG log-conformation formulation

The DEVSS-TG/SUPG log-conformation formulation, which has $\mathbf{v}$, p, $\mathbf{L}$ and $\mathbf{S}$ as unknowns, is obtained by solving Eq. (10) coupled with Eqs. (1)–(3) (as in DEVSS-TG/SUPG) in the laboratory frame. The weighted residual equations are given by

$$\int_\Omega \nabla\mathbf{w} : \mathbf{T}\,\mathrm{d}\Omega + \int_\Gamma \mathbf{w}\cdot\mathbf{h}\,\mathrm{d}\Gamma = \mathbf{0}, \tag{11}$$

$$\int_\Omega q(\nabla\cdot\mathbf{v})\,\mathrm{d}\Omega = 0, \tag{12}$$

$$\int_\Omega \mathbf{E} : \left[\mathbf{L} - \nabla\mathbf{v} + \frac{1}{\mathrm{tr}\,\mathbf{I}}(\nabla\cdot\mathbf{v})\mathbf{I}\right]\,\mathrm{d}\Omega = \mathbf{0}, \tag{13}$$

$$\int_\Omega \left[\mathbf{R} + h^u\mathbf{v}\cdot\nabla\mathbf{R}\right] : \left[-\mathbf{v}\cdot\nabla(\exp\mathbf{S}) + 2\xi\frac{\mathbf{D}:(\exp\mathbf{S})}{\mathbf{I}:(\exp\mathbf{S})}(\exp\mathbf{S}) + \zeta\left((\exp\mathbf{S})\cdot\mathbf{D} + \mathbf{D}\cdot(\exp\mathbf{S}) - 2\frac{\mathbf{D}:(\exp\mathbf{S})}{\mathbf{I}:(\exp\mathbf{S})}(\exp\mathbf{S})\right) + (\exp\mathbf{S})\cdot\mathbf{W} + \mathbf{W}^T\cdot(\exp\mathbf{S}) - \frac{1}{\lambda}(g_0\mathbf{I} + g_1(\exp\mathbf{S}) + g_2(\exp\mathbf{S})^2)\right]\,\mathrm{d}\Omega = \mathbf{0}, \tag{14}$$

where $\mathbf{w}$, q, $\mathbf{E}$ and $\mathbf{R}$ are the weighting functions multiplying the conservation of momentum, continuity, traceless velocity gradient and constitutive equations, respectively, and h^u is the characteristic element length used by the SUPG stabilization of the constitutive equation.

The Galerkin method is used to discretize the governing equations; therefore, the weighting functions are considered to be the

same as the test functions used to approximate the variables (except for the conformation equation, which uses streamupwind Petrov-Galerkin as in Ref. [7]). Bilinear piecewise continuous functions are used for p, $\mathbf{L}$ and $\mathbf{S}$, whereas biquadratic functions for $\mathbf{v}$. In this case, the variable $\mathbf{S}$ grows roughly linearly or sub-linearly in regions of strong flow, removing problems associated with the poor representation by low-order polynomial interpolation functions of $\mathbf{M}$, which has an exponential behavior in strong flow regions.

4.2. Numerical issues associated with the implementation of the log-conformation formulation

4.2.1. Computation of $\exp \boldsymbol{S}$ and $\nabla(\exp \boldsymbol{S})$

The transformation in Eq. (14) is not done explicitly; rather, $\mathbf{M} = \exp \mathbf{S}$ is computed at each Gauss point where the weighted residual must be evaluated. The $\exp \mathbf{S}$ is calculated by using spectral decomposition,

$$\mathbf{S} = \mathbf{V}\boldsymbol{\Sigma}\mathbf{V}^{-1}, \tag{15}$$

where each column of $\mathbf{V}$ is an eigenvector of $\mathbf{S}$, and $\boldsymbol{\Sigma}$ is a diagonal matrix whose elements are the eigenvalues of $\mathbf{S}$; therefore,

$$\exp \mathbf{S} = \mathbf{V}(\exp \boldsymbol{\Sigma})\mathbf{V}^{-1}, \tag{16}$$

where $\exp \boldsymbol{\Sigma}$ is obtained by taking the exponential of each element of the diagonal matrix $\boldsymbol{\Sigma}$. The eigenvalues and eigenvectors of $\mathbf{S}$ are found analytically in 2-D.

Whereas $\exp \mathbf{S}$ can be obtained straightforwardly, $\nabla(\exp \mathbf{S})$ in Eq. (10) cannot be computed easily; thus, an approximation is used. Three different ways to do so are presented here:

(1) By computing $\mathbf{M}^\alpha = \exp \mathbf{S}^\alpha$ at every node, and multiplying by the derivative of the basis function $\varphi_{\mathbf{S}}$ used to approximate $\mathbf{S} \equiv \sum_\alpha \mathbf{S}^\alpha \varphi^\alpha_{\mathbf{S}}$,

$$\nabla(\exp \mathbf{S}) = \nabla \mathbf{M} \approx \sum_\alpha (\nabla \varphi^\alpha_{\mathbf{S}})\mathbf{M}^\alpha, \tag{17}$$

where α is a dummy index from 1 to the number of basis functions for approximating $\mathbf{S}$;

(2) By using finite differences. In this case, $\mathbf{S}(\xi, \eta) \equiv \sum_\alpha \mathbf{S}^\alpha \varphi^\alpha_{\mathbf{S}}(\xi, \eta)$ is computed at the points $(\xi + \varepsilon, \eta)$, $(\xi - \varepsilon, \eta)$, $(\xi, \eta + \varepsilon)$, and $(\xi, \eta - \varepsilon)$ in the local co-ordinate system (ξ, η) and then $\mathbf{M}(\xi, \eta) = \exp \mathbf{S}(\xi, \eta)$ is calculated at every point. Therefore, the components of $\nabla(\exp \mathbf{S}) = \nabla \mathbf{M}$ are obtained from:

$$\frac{\partial M_{ij}}{\partial \xi} \approx \frac{M_{ij}(\xi + \varepsilon, \eta) - M_{ij}(\xi - \varepsilon, \eta)}{2\varepsilon}, \tag{18}$$

$$\frac{\partial M_{ij}}{\partial \eta} \approx \frac{M_{ij}(\xi, \eta + \varepsilon) - M_{ij}(\xi, \eta - \varepsilon)}{2\varepsilon}, \tag{19}$$

where $\varepsilon = 10^{-6}$;

(3) By expressing the convective term by means of the gradient of $\mathbf{S}$ rather than the gradient of $\mathbf{M}$, for a better convective stability,

$$-\mathbf{v} \cdot \nabla(\exp \mathbf{S}) = \lim_{h^* \to 0} \frac{\exp(\mathbf{S} - h^* \mathbf{v} \cdot \nabla \mathbf{S}) - \exp(\mathbf{S})}{h^*}, \tag{20}$$

where h^* is a numerical parameter. Hereafter, we use $h^* = 10^{-6} h^u$ to balance transition versus finite precision error (here h^u is the length of an element).

Unless otherwise stated, the first approximation is used in most of the simulations. After computing the basic variables—$\mathbf{v}$, p, $\mathbf{L}$ and $\mathbf{S}$—the conformation field $\mathbf{M}$ is obtained from $\mathbf{S}$ at every node by Eq. (16).

4.2.2. Imposing boundary conditions on $\boldsymbol{S}$

Whereas imposing boundary conditions on $\mathbf{v}$ and p is straightforward, imposing boundary conditions on $\mathbf{S}$ is not trivial because it requires solving the fully developed flow condition of Eq. (10) analytically. This could be tedious for complex constitutive equations for which a simple expression cannot be derived. However, a remedy for this problem was presented by Xie and Pasquali [11], where the constitutive equation, given by Eq. (10), is also solved numerically at all the inflow boundaries; in this case, the fully developed boundary condition is imposed by setting $\mathbf{v} \cdot \nabla(\exp \mathbf{S}) = \mathbf{0}$.

4.2.3. Mixed Jacobian matrix

Newton's method is used to solve the nonlinear algebraic equation set arising from the discretization of the governing equations. The analytical derivatives of the problem equations with respect to $\mathbf{S}$ are not known. Thus, a mixed Jacobian matrix is used; analytical for the derivatives with respect to $\mathbf{v}$, p and $\mathbf{L}$, and numerical for the derivatives with respect to $\mathbf{S}$. The latter is obtained by central finite difference,

$$\mathbf{J}(:, j) = \frac{\mathbf{r}(x_j + \varepsilon) - \mathbf{r}(x_j - \varepsilon)}{2\varepsilon}, \tag{21}$$

where $\mathbf{J}$ is the Jacobian matrix, $\mathbf{r}$ the residual vector, x_j the unknowns (in this case only the components of $\mathbf{S}$) and ε is the imposed perturbation. Computationally, the numerical Jacobian is more expensive than the analytical one; therefore, a complete analytical Jacobian would be preferable.

5. Numerical results

The effectiveness of the DEVSS-TG/SUPG log-conformation formulation is demonstrated for the Oldroyd-B model in the complex problem of flow past a cylinder in a rectangular channel in the case where the ratio of half channel width to the cylinder radius is 2:1. Details of the geometry, boundary conditions, finite element meshes, and more complete references are reported in Ref. [10].

5.1. Oldroyd-B model

The Oldroyd-B model is given by the constitutive parameters $\xi = 1, \zeta = 1, g_0 = -1, g_1 = 1$, and $g_2 = 0$, and the elastic stress

Table 1
Flow past a cylinder in a channel of an Oldroyd-B fluid: finite element meshes and drag forces at different Wi

Mesh	Elements	Drag force at different Wi				
		0.6	0.7	0.8	0.9	1.0
M1	4,788	117.97	177.56	177.62	118.06	118.81
M2	8,512	117.88	117.44	117.47	117.86	118.54
M3	13,300	117.84	117.39	117.41	117.78	118.43

is related to the conformation tensor as

$$\boldsymbol{\sigma} = G\mathbf{M}, \tag{22}$$

where $G = \eta_p/\lambda$ is the elastic modulus, and η_p is the polymer contribution to the viscosity. A viscosity ratio of $\beta = \eta_s/(\eta_s + \eta_p) = 0.59$ is used in all our simulations. The drag on the cylinder f_d is calculated as,

$$f_d = -2\int_S \mathbf{e}_1\mathbf{n} : \mathbf{T}\,\mathrm{d}S, \tag{23}$$

where S represents the surface of the cylinder, $\mathbf{n}$ is the unit normal vector, and $\mathbf{e}_1$ is the unit vector in the x-direction. Table 1 shows the values of the drag force at different Wi, and Fig. 1 plots these values with the values reported in Ref. [5]; good agreement is observed.

Although mesh-converged solution for the drag force—an integral quantity over the cylinder—is observed in Fig. 1, this does not guarantee the accuracy and convergence of the solution in the entire domain. Figs. 2–4 show the elastic stress $\sigma_{xx} = (\eta_p/\lambda)M_{xx}$ versus s ($0 < s < \pi R_c$ on the cylinder and $\pi R_c < s < \pi R_c + L_d - R_c$ in the wake along the symmetry line, where R_c is the cylinder radius and L_d the downstream length). Fig. 2 shows the results for the three meshes at Wi = 0.6; a complete overlap is observed. The results are also in good agreement with Ref. [5].

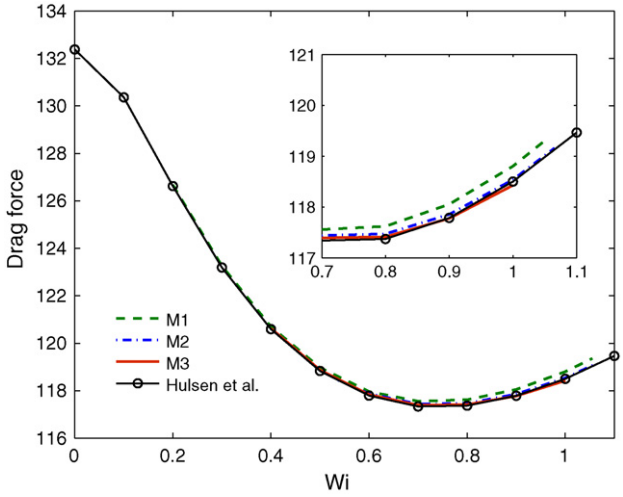

Fig. 1. Flow past a cylinder in a channel of an Oldroyd-B fluid: drag force on the cylinder versus Wi. The DEVSS-TG/SUPG log-conformation results for the three meshes (M1, M2 and M3) are compared with the results presented by Hulsen et al. [5]. Inset: detail of the drag force at high Wi.

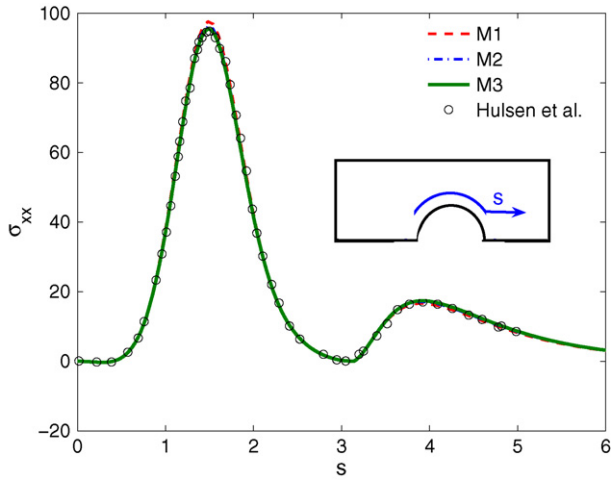

Fig. 2. Flow past a cylinder in a channel of an Oldroyd-B fluid: σ_{xx} on the cylinder and on the symmetry line in the wake. (○) From Hulsen et al. [5]. Wi = 0.6.

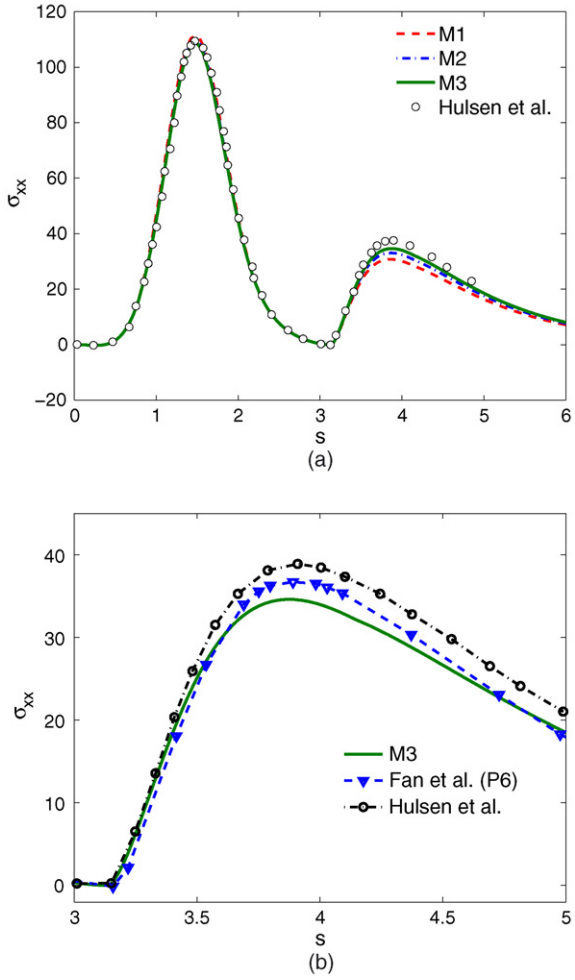

Fig. 3. Flow past a cylinder in a channel of an Oldroyd-B fluid: (a) σ_{xx} on the cylinder and on the symmetry line in the wake; (b) σ_{xx} on the symmetry line in the wake. (○) From Hulsen et al. [5] and (▽) From Fan et al. [12] for P6 (using polynomial interpolation functions of order 6). Wi = 0.7.

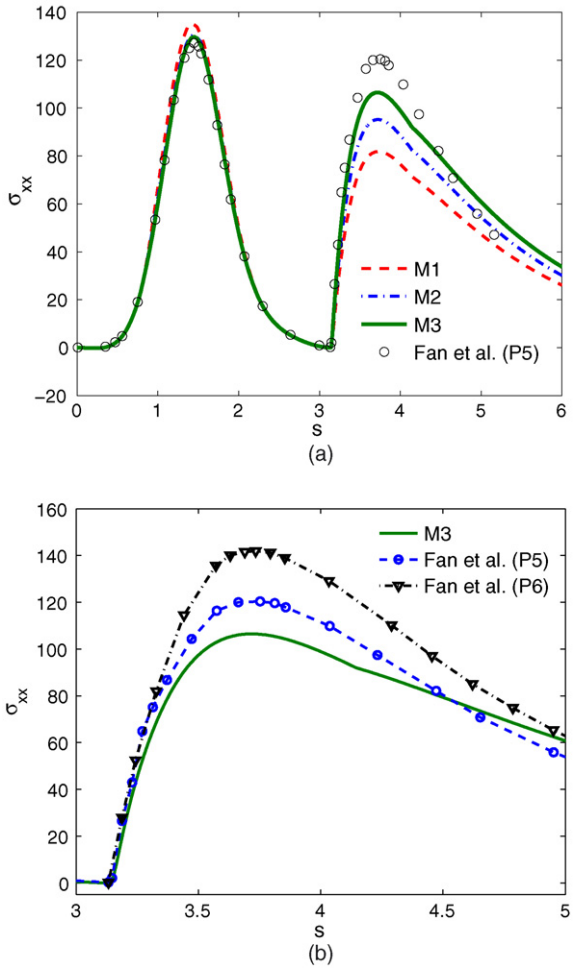

Fig. 4. Flow past a cylinder in a channel of an Oldroyd-B fluid: (a) σ_{xx} on the cylinder and on the symmetry line in the wake; (b) σ_{xx} on the symmetry line in the wake. (○) From Fan et al. [12] for P5 and (▽) from Fan et al. [12] for P6 (using polynomial interpolation functions of order 5 and 6, respectively). Wi = 0.9.

At Wi = 0.7, the results agree well on the cylinder, but differences are observed in the wake flow; Fig. 3(a) shows σ_{xx} for the different meshes, and Fig. 3(b) compares the result on the fine mesh (M3) with published results by Hulsen et al. [5] and Fan et al. [12] (for a polynomial interpolation function of order 6 (P6)).

Fig. 4(a) shows the results at Wi = 0.9 where no sign of mesh convergence is observed as already reported in the literature [5,12], and Fig. 4(b) compares the result on the fine mesh (M3) with published results by Fan et al. [12] using polynomial interpolation functions of order 5 and 6 (P5 and P6, respectively); the numerical values of σ_{xx} continue to grow with mesh refinement. Whereas, the simulations remain stable at high Wi, accuracy is lost after a critical Wi $\sim$ 0.7 (as also observed in Refs. [5,12]).

We study convergence further by examining the convergence of M_{xx} at $x = 2(s = \pi + 1)$, $y = 0$; this location is chosen because it is the place where the largest differences are observed. Richardson extrapolation is used to analyze the convergence of

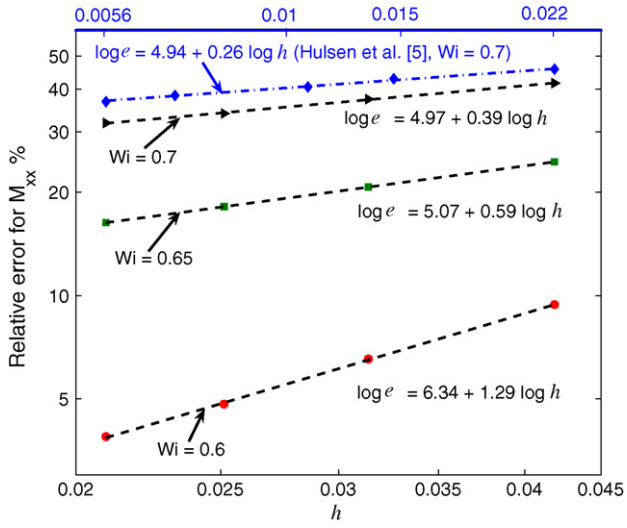

Fig. 5. Flow past a cylinder in a channel of an Oldroyd-B fluid: mesh-convergence rate of M_{xx} ($x = 2$, $y = 0$) at Wi = 0.6, 0.65 and 0.7. (⧫) From the data provided by Hulsen et al. [5] at Wi = 0.7 (top axis).

M_{xx} with mesh refinement,

$$M_{xx}(0) = M_{xx}(h) + \alpha h^n, \tag{24}$$

where $M_{xx}(0)$ is M_{xx} for an infinitely refined mesh, h the element length, n the rate of mesh convergence and α is a constant. After fitting the data using Eq. (24), $M_{xx}(0)$ is used to calculate the relative errors

$$e = \left| \frac{M_{xx}(h) - M_{xx}(0)}{M_{xx}(0)} \right| \times 100\%. \tag{25}$$

The relative errors at Wi = 0.6, 0.65 and 0.7 against h are plotted in Fig. 5 using a log–log scale, where the slopes are given by n. At Wi = 0.6, a rate of mesh convergence of $n = 1.29$ is attained. Even though $n < 1$ for Wi > 0.6, the relative errors are still decreasing with mesh refinement but very slowly ($n = 0.59$ and 0.39 for Wi = 0.65 and 0.7, respectively), which means that with the meshes used in this work, we are still not in the terminal mesh convergence range; therefore, more refined meshes are required to come to any conclusion. The same analysis is performed with the data provided by Hulsen et al. [5] (also plotted in Fig. 5) obtaining a rate of mesh convergence of $n = 0.26$ at Wi = 0.7 (using more refined meshes), which is slightly lower than the one obtained in this work.

Fig. 6 shows the contour plots of the components of **M** at Wi = 1.0 on M3. Clearly, although the solution in the wake is not mesh converged, the contour lines are more regular than those obtained in Ref. [10] at lower Wi = 0.7 on a similar mesh.

5.2. Results at high Wi

First-order arc-length continuation with automatic step control on Wi is applied to compute the flow states; the continuation terminates when the residual norm cannot be decreased below 10^{-5} (10^{-4} for Wi > 1). The simulation on the three meshes stop at Wi $\sim$ 1.05; in comparison to the traditional

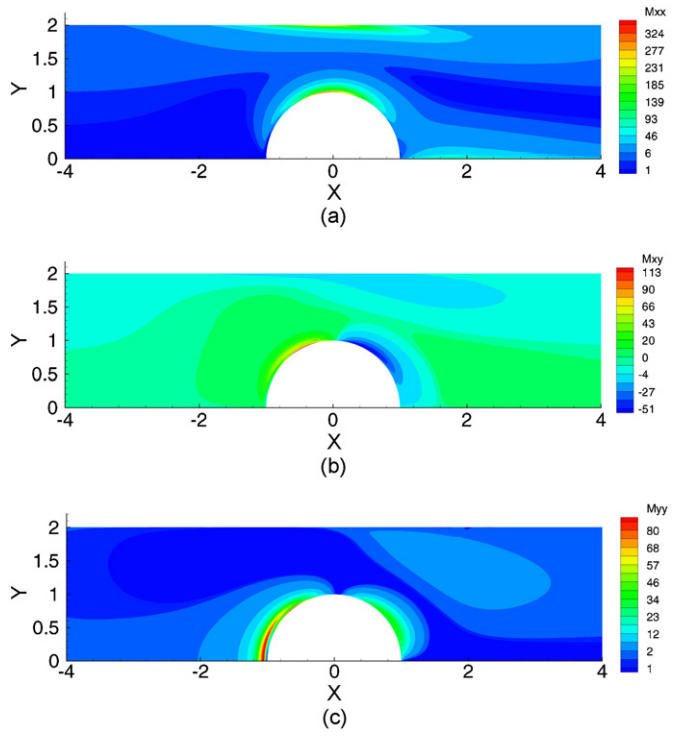

Fig. 6. Flow past a cylinder in a channel of an Oldroyd-B fluid: (a) M_{xx}; (b) M_{xy}; (c) M_{yy} contours at Wi = 1.0 on mesh M3.

DEVSS-TG/SUPG [7], it represents an increase of about 40% in the maximum Wi. If the alternative approximations of $\nabla(\exp \mathbf{S})$ and $\mathbf{v} \cdot \nabla(\exp \mathbf{S})$, given in Section 4.2.1 are used, an increase of about 20% in the maximum Wi is observed. Although the third way to approximate the convective term should have better stability, it performs as the second one.

Fig. 7 plots the residual norm against the number of iterations at Wi = 0.83, 0.92, 1.05, and 1.07 (near to the maximum Wi). A quadratic rate of reduction of the residual norm is expected by the Newton's method; in this case, the rate of convergence

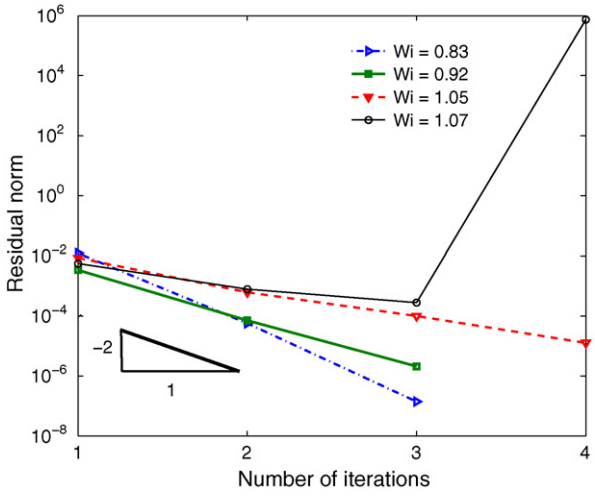

Fig. 7. Residual norm versus number of Newton iterations at high Wi (close to the maximum Wi). A slope of two (expected for Newton's method) is drawn to guide the eye.

drops and the minimum attainable residual norm grows larger as Wi increases above Wi ≈ 0.9; Newton's method breaks down altogether at Wi = 1.07.

The maximum Wi obtained by Hulsen et al. [5] with a different log-conformation formulation in finite element context was Wi = 1.8 (maximum Wi obtained here is Wi ≈ 1.05). This difference and the issues discussed in the previous paragraphs are considered in the next section, where the performance of these two formulations are studied in a simple 1-D problem.

6. 1-D analysis

We analyze the performance of the log-conformation formulations presented in Ref. [5] (*method 1*) against the one proposed in this work (*method 2*). For this, we study the prototypical 1-D convection-generation equation

$$\frac{\mathrm{d}m}{\mathrm{d}x} - \alpha m = 0, \tag{26}$$

where $m(x)$ ($x \in [0, 1]$) is the unknown and $\alpha > 0$ is parameter controlling the rate of exponential growth of the solution. The boundary condition of the problem is $m(0) = 1$, and it has the exact solution $m^a = \exp(\alpha x)$. Both methods are solved using the SUPG formulation.

6.1. Method 1

This method mimics the approach followed by Hulsen et al. [5] (also reviewed in Section 3). Here, Eq. (26) is transformed by using the variable $s = \log m$ as

$$\frac{\mathrm{d}s}{\mathrm{d}x} - \alpha = 0, \tag{27}$$

where the variable s is approximated by using linear basis functions ϕ_i. The residual vector is

$$r_i = \int_0^1 w_i \left[\frac{\mathrm{d}s}{\mathrm{d}x} - \alpha\right] \mathrm{d}x, \tag{28}$$

where i varies from 1 to the number of basis functions, and w_i is the weight function, which for the case of the SUPG method, is given by

$$w_i = \phi_i + h\frac{\mathrm{d}\phi_i}{\mathrm{d}x}, \tag{29}$$

where h is the element length. This discretization gives a linear problem; therefore, it is solved in one iteration with Newton's method.

6.2. Method 2

This method mimics the approach presented in Section 4. Here, Eq. (26) is unchanged; however, whenever the variable m is present, it is replaced by $\exp(s)$, and s is approximated with

linear basis functions. The residual vector is

$$r_i = \int_0^1 w_i \left[\exp(s) \frac{\mathrm{d}s}{\mathrm{d}x} - \exp(s)\alpha \right] \mathrm{d}x. \tag{30}$$

This is a non-linear problem; therefore, a good initial guess is required for Newton's method in order to converge to a solution.

6.3. Results of the 1-D analysis

The results for $\alpha = 24$ are shown in Fig. 8. Fig. 8(a) plots the analytical results along with the numerical results obtained by *methods 1* and *2* against x and Fig. 8(b) plots the relative errors e of the two methods against x, where

$$e = \left| \frac{m^a - m}{m^a} \right| 100\%. \tag{31}$$

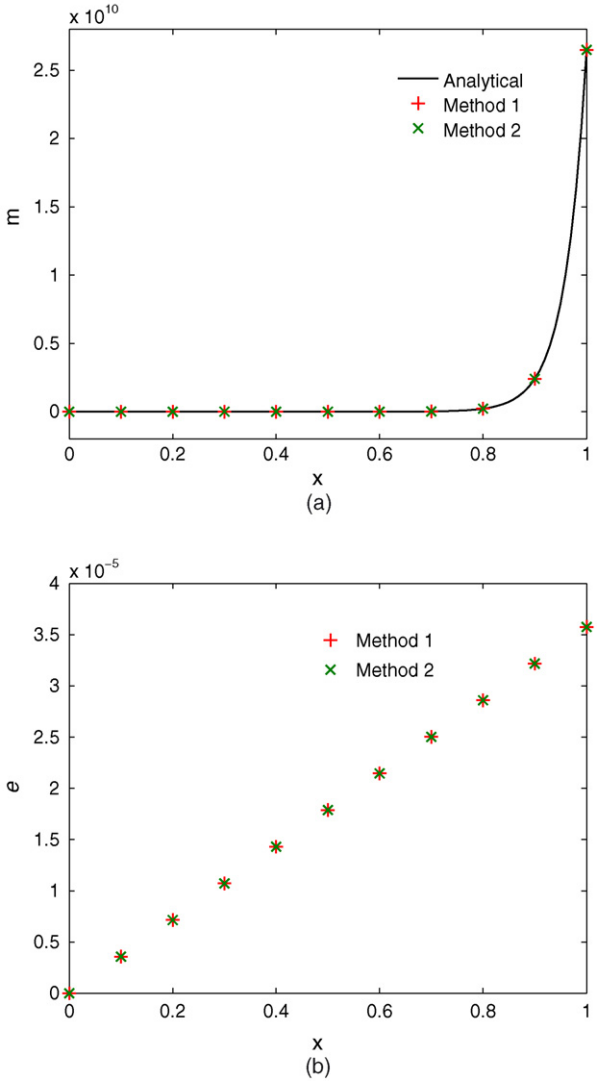

Fig. 8. 1-D analysis, $\alpha = 24$: (a) numerical results obtained by the *methods 1* and *2* compared with the analytical ones; (b) relative errors with respect to the analytical solution.

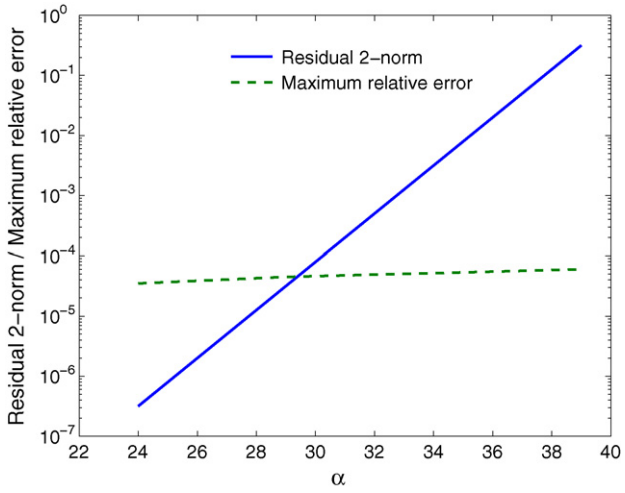

Fig. 9. Residual 2-norm and maximum relative error against α for the *method 2*.

As can be seen in Fig. 8, there is no apparent difference in the results obtained by the two methods and this trend continues for even higher α. As expected, the maximum relative error is obtained at $x = 1$.

However, the minimum 2-norm residual that can be obtained by *method 2* depends on α, which keeps oscillating after certain value no matter the number of Newton's iterations allowed. For instance, this minimum is between 10^{-7} and 10^{-6}, 10^{-5} and 10^{-4}, and 10^{-1} and 10^{0} for $\alpha = 24$, 29, and 39, respectively. As can be noticed, the minimum norm increases considerably as α is increased; therefore, in order to accept a solution, the maximum error allowed by the Newton's method is increased accordingly. In all cases, quadratic convergence is observed until the minimum norm is attained.

It can be noticed from Fig. 9 that even though the residual norms are high for high values of α, the relative errors are small and increase very slowly with α. The same trend is also observed in our simulations using the DEVSS-TG/SUPG log-conformation formulation at high Wi, as previously described in Section 5.2. This behavior can be explained by considering Eq. (30), where the residual vector is multiplied by the factor $\exp(s)$ ($\exp \mathbf{S}$ in Eq. (14)), which grows exponentially as α (Wi) increases. At high α (Wi), the numerical precision of the calculations approach the machine precision limit; therefore, accurate numerical solutions after a critical value of α (Wi) are difficult to obtain. This may explain why the residual norm cannot be decreased any further in simulations close to this critical value, as also observed in our 2-D simulations.

7. Demonstration of the generality of the DEVSS-TG/SUPG log-conformation formulation

The advantages of the log-conformation formulation presented in this paper are its generality and straight forward implementation. It can be easily applied to solve for any constitutive model in terms of the conformation tensor Eq. (4), without requiring code modifications. Its generality is demonstrated by

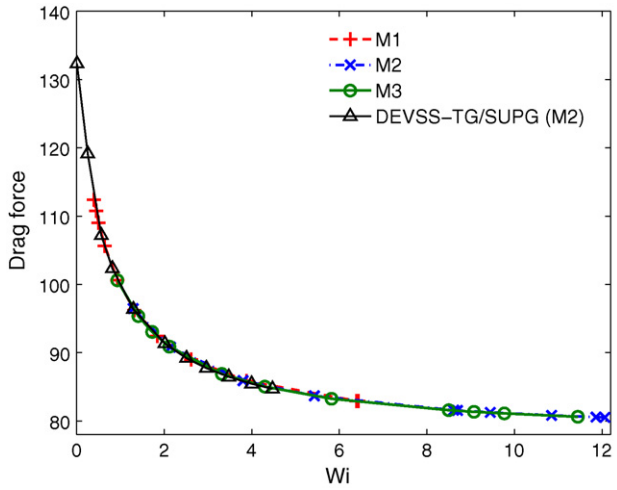

Fig. 10. Flow past a cylinder in a channel of a Larson-1 fluid (Eq. (54b) of Ref. [18]) with $\bar{\zeta} = 0.05/3$, $\beta = 0.59$: drag force on the cylinder versus Wi for the three meshes (M1, M2 and M3) using the DEVSS-TG/SUPG log-conformation formulation, and compared with the results obtained by the original DEVSS-TG/SUPG formulation on M2.

using models with affine and non-affine deformation. Constitutive models of affinely deforming fluids are obtained when $\xi = \zeta = 1$, e.g., Oldroyd-B [13], Giesekus [14], Leonov [15], FENE-type [16,17], and Larson-1 [18] models, whereas fluids with non-affine microstructure deformations are obtained when $\xi < 1$ or $\zeta < 1$, e.g., PTT-type [19,20], Johnson-Segalman [21], and Larson-2 to Larson-4 [18] models.

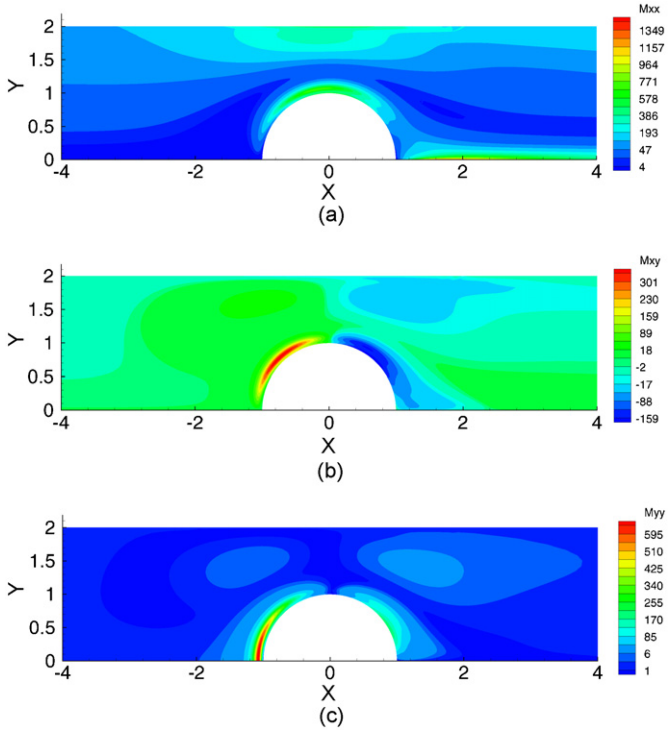

Fig. 11. Flow past a cylinder in a channel of a Larson-1 fluid: (a) M_{xx}; (b) M_{xy}; (c) M_{yy} contours at Wi = 11.4 on mesh M3.

7.1. Larson-1 model

For the case of constitutive models considering affine deformations, the flow of a Larson-1 fluid (Eq. (54b) of Ref. [18]) past a cylinder in a rectangular channel is considered. This model is selected because the relaxation functions are not constant as in the case of the Oldroyd-B model. The constitutive parameters of the Larson-1 model are $\xi = 1$, $\zeta = 1$, $g_0 = -1 - \bar{\zeta}(I_M - 3)$, $g_1 = 1 + \bar{\zeta}(I_M - 3)$, and $g_2 = 0$, where $\bar{\zeta}$ is a constant, and $I_M = \mathrm{tr}(\mathbf{M})$ is the first invariant of $\mathbf{M}$. The elastic stress is related to the conformation tensor as

$$\boldsymbol{\sigma} = \frac{G}{1 + \bar{\zeta}(I_M - 3)}\mathbf{M}. \tag{32}$$

Fig. 10 plots the drag force against Wi in the case for $\bar{\zeta} = 0.05/3$ and $\beta = 0.59$. The highest Wi attained in these simulations are 6.4, 12.3, and 11.4 on M1, M2 and M3, respectively; a complete overlap is observed. Because no published results are available for this problem, the results are compared with the solutions obtained by the original DEVSS-TG/SUPG formulation on M2, also plotted in Fig. 10. In this case, the simulations stopped at Wi $\approx$ 4.49, which indicates that an increase of nearly a factor of 3 in the maximum Wi can be obtained by using the DEVSS-TG/SUPG log-conformation formulation on the same mesh.

Fig. 11 shows the contour plots of the components of $\mathbf{M}$ at the maximum Wi = 11.4 on M3.

7.2. Larson-2 model

For the case of constitutive models with non-affine deformation, the flow of a Larson-2 fluid (Eq. (54a) of Ref. [18]) past a cylinder in a rectangular channel is considered. The Larson-2 model is given by the constitutive parameters $\xi = \bar{\xi}$, $\zeta = 1$, $g_0 = -1$, $g_1 = 1$, and $g_2 = 0$, where $\bar{\xi}$ is a constant, and the

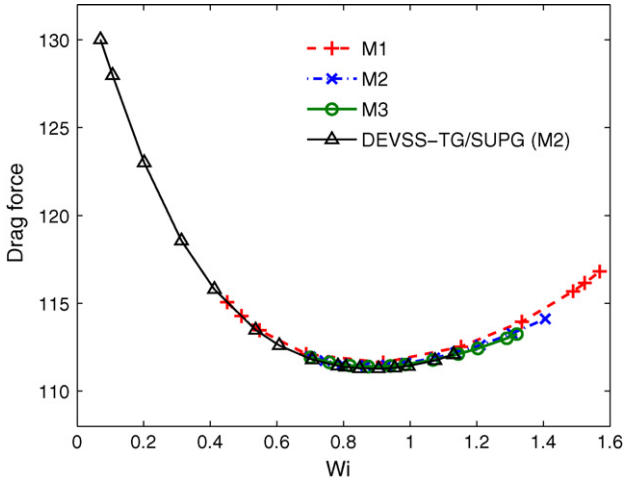

Fig. 12. Flow past a cylinder in a channel of a Larson-2 fluid (Eq. (54a) of Ref. [18]) with $\xi = 0.9$: drag force on the cylinder versus Wi for the three meshes (M1, M2 and M3) using the DEVSS-TG/SUPG log-conformation formulation, and compared with the results obtained by the original DEVSS-TG/SUPG formulation on M2.

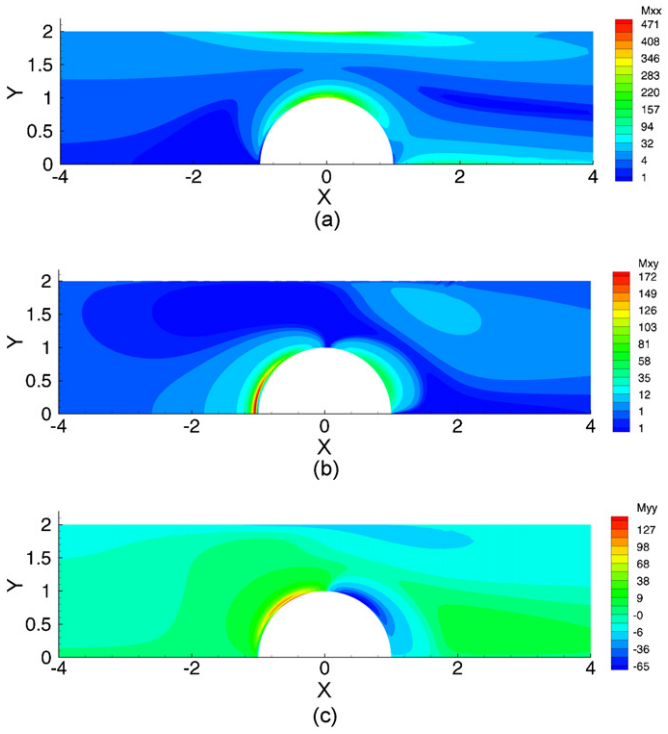

Fig. 13. Flow past a cylinder in a channel of a Larson-2 fluid: (a) M_{xx}; (b) M_{xy}; (c) M_{yy} contours at Wi = 1.32 on mesh M3.

relation between $\boldsymbol{\sigma}$ and $\mathbf{M}$ is given by Eq. (22) (same as for the Oldroyd-B model).

Fig. 12 plots the drag force against Wi in the case $\xi = 0.9$ and $\beta = 0.59$. The highest Wi obtained in our simulation are 1.56, 1.41 and 1.32 on M1, M2 and M3, respectively. The results on M1 are slightly above the results obtained on M2 and M3, which are in good agreement. As in the previous case, no published results are available in the literature; they are compared with the results obtained by the DEVSS-TG/SUPG formulation on M2, shown in Fig. 12. An increase of the maximum Wi of about 24% is obtained by using the DEVSS-TG/SUPG log-conformation formulation on the same mesh.

Fig. 13 shows the contour plots of the components of $\mathbf{M}$ at the maximum Wi = 1.32 on M3.

8. Conclusions and discussions

A simple alternate implementation for the log-conformation formulation is presented in this article. The implementation is demonstrated in the finite element context, and a DEVSS-TG/SUPG log-conformation method is proposed. In comparison to the previous works on log-conformation formulation [3,5,6], the new implementation requires even fewer code modifications, and has the advantage of solving all governing equations in a coupled way in a laboratory co-ordinate frame. Effectively, this new implementation retains the set of governing equations, and uses the matrix-logarithm as a basis function for the conformation field which evolve exponentially near the boundaries. Additionally, in order to try to understand the difference observed between the different ways of implementing the log-conformation formulation, a 1-D analysis is presented.

The method is used to simulate flow of several viscoelastic fluids modeled by generalized constitutive model in the benchmark problem of flow past a cylinder in channel. The Oldroyd-B and Larson-1 models consider affine deformation for the polymer constituents, whereas the Larson-2 model considers non-affine deformation. It is demonstrated that the method works well for the generalized constitutive model, and improves the numerical stability at high Wi. In the flow past a cylinder in a channel of an Oldroyd-B fluid problem, the maximum Wi limit was extended to 1.05 as compared to 0.75 obtained with the original DEVSS-TG/SUPG method, although mesh-converged solutions were not demonstrated for Wi > 0.6. For the Larson-1 model was extended from 4.49 to 12.30 and for the Larson-2 model from 1.13 to 1.41, both on M2.

The results from the DEVSS-TG/SUPG log-conformation are found to be promising, although there are still two issues associated with the implementation that must be resolved in future work. First, a more accurate approximation for $\nabla(\exp \mathbf{S})$ should be obtained; this will improve the limit up to which the Newton's method will remain convergent. Second, a complete analytical Jacobian for the Newton's method should be derived; this will reduce the high computational cost associated with the numerical Jacobian.

Acknowledgments

We thank Raz Kupferman for discussions and suggesting the third way to approximate the convective term given in the Eq. (20), Michael Renardy and Martien Hulsen for valuable discussions (MH also for providing mesh convergence data from his work). This work was supported by the National Science Foundation under awards CTS-ITR-0312764 and CTS-CAREER 0134389, and the German Science Foundation under SFB 540, SPP 1253 and GSC 111 (AICES) programs. Additional support was provided by Micromed Cardiovascular, Inc. Computational resources were provided by the Rice Terascale Cluster funded by NSF (EIA-0216467), Intel, and Hewlett-Packard, and the Rice Cray XD1 Research Cluster funded by NSF (CNS-0421109), AMD, and Cray. Additional computing resources were provided by the RWTH Aachen Center for Computing and Communication and by the Forschungszentrum Jülich.

References

[1] A.N. Beris, B.J. Edwards, Thermodynamics of Flowing Systems with Internal Microstructure, 1st ed., Oxford University Press, Oxford, 1994.
[2] M. Renardy, A comment on smoothness of viscoelastic stresses, J. Non-Newtonian Fluid Mech. 138 (2006) 204–205.
[3] R. Fattal, R. Kupferman, Constitutive laws for the matrix-logarithm of the conformation tensor, J. Non-Newtonian Fluid Mech. 123 (2004) 281–285.
[4] R. Fattal, R. Kupferman, Time-dependent simulation of viscoelastic flows at high Weissenberg number using the log-conformation representation, J. Non-Newtonian Fluid Mech. 126 (2005) 23–37.
[5] M.A. Hulsen, R. Fattal, R. Kupferman, Flow of viscoelastic fluids past a cylinder at high Weissenberg number: stabilized simulations using matrix logarithms, J. Non-Newtonian Fluid Mech. 127 (2005) 27–39.
[6] Y. Kwon, Finite element analysis of planar 4:1 contraction flow with the tensor-logarithmic formulation of differential constitutive equation,

Korea–Australia. Rheol. J. 16-4 (2004) 183–191.
[7] M. Pasquali, L.E. Scriven, Free surface flows of polymer solutions with models based on the conformation tensor, J. Non-Newtonian Fluid Mech. 108 (2002) 363–409.
[8] M. Pasquali, L.E. Scriven, Theoretical modeling of microstructured liquids: a simple thermodynamic approach, J. Non-Newtonian Fluid Mech. 120 (2004) 101–135.
[9] R.I. Tanner, Engineering Rheology, 2nd ed., Oxford University Press, Oxford, 2000.
[10] O.M. Coronado, D. Arora, M. Behr, M. Pasquali, Four-field Galerkin/least-squares formulation for viscoelastic flows, J. Non-Newtonian Fluid Mech. 140 (2006) 132–144.
[11] X. Xie, M. Pasquali, A new, convenient way of imposing open-flow boundary conditions in two- and three-dimensional viscoelastic flows, J. Non-Newtonian Fluid Mech. 122 (2004) 159–176.
[12] Y. Fan, R.I. Tanner, N. Phan-Thien, Galerkin/least-square finite-element methods for steady viscoelastic flows, J. Non-Newtonian Fluid Mech. 84 (1999) 233–256.
[13] J.G. Oldroyd, On the formulation of rheological equations of state, Proc. Royal Soc. Lond. A 200 (1950) 523–541.
[14] H. Giesekus, A simple constitutive equation for polymer fluids based on the concept of deformation-dependent tensorial mobility, J. Non-Newtonian Fluid Mech. 11 (1982) 69–109.
[15] A.I. Leonov, Nonequilibrium thermodynamics and rheology of viscoelastic polymer media, Rheol. Acta 25 (1976) 85–98.
[16] R.B. Bird, C.F. Curtiss, R.C. Armstrong, O. Hassager, Dynamics of Polymeric Liquids, vol. 2, 2nd ed., John Wiley & Sons, New York, 1987.
[17] M.D. Chilcott, J.M. Rallison, Creeping flow of dilute polymer solutions past cylinders and spheres, J. Non-Newtonian Fluid Mech. 29 (1988) 381–432.
[18] R.G. Larson, A constitutive equation for polymer melts based on partially extending strand convection, J. Rheol. 28 (1984) 545–571.
[19] N. Phan-Thien, R.I. Tanner, A new constitutive equation derived from network theory, J. Non-Newtonian Fluid Mech. 2 (1977) 353–365.
[20] N. Phan-Thien, A nonlinear network viscoelastic model, J. Rheol. 22 (1978) 259–283.
[21] M.D. Johnson, D. Segalman, A model for viscoelastic fluid behavior which allows non-affine deformation, J. Non-Newtonian Fluid Mech. 2 (1977) 225–270.